Synthesis, Structure and Magnetic Properties of Chiral Molecule-Based Magnets[*]

Jun-ichiro Kishine,[1,**] Katsuya Inoue[2,***] and Yusuke Yoshida[2,†]

[1]*Department of Physics, Faculty of Engineering, Kyushu Institute of Technology, Kitakyushu 804-8550, Japan*
[2]*Department of Chemistry, Faculty of Science, Hiroshima University, Higashi-Hiroshima 739-8526, Japan*

In this paper, we discuss the origin of magnetic chirality of chiral magnets made by chromium (III) and manganese (II) ions. Structurally characterized yellow needles: $K_{0.4}[Cr(CN)_6][Mn(S)\text{-pn}](S)\text{-pnH}_{0.6}$ ((S)-pn = (S)-1,2-diaminopropane) and green needles: $[Cr(CN)_6][Mn(S \text{ or } R)\text{-pnH}(H_2O)]H_2O$ were obtained by the reaction among $K_3[Cr(CN)_6]$, $Mn(ClO_4)_2$, (R or S)-pn·2HCl and KOH. The space groups of green needle and yellow needle are $P2_12_12_1$ and $P6_1$, respectively. From the X-ray crystallographic analysis of them, the yellow needle has three-dimensional and green needle has two-dimensional magnetic connectivity. These ferrimagnets are good candidates for chiral spin order at low temperature. We present some theoretical supports, within classical phenomenologies, to understand characteristic features of the chiral magnetic materials and their magnetic properties.

§1. Introduction

Molecular chemistry in principle can fine tune the structures and the properties of complex aggregates, and nature already provides a large number of molecular aggregates which can perform the most disparate functions. Especially, because molecule-based materials are transparent for the light, in recent years optical properties of them have attracted much attention. Specific goals for these molecule-based magnets include the rational design of a magnet having i) a desired geometrical structure and/or dimensionality and ii) an optical transparency.[1),2)] The physical characteristics of current interest involve optical properties, particularly with respect to natural optical activity. In the case of a magnet with non-centrosymmetric structure, the space-inversion ($\mathcal{P}$) and time-reversal ($\mathcal{T}$) symmetry are simultaneously broken. Moreover, when a magnet is characterized by chiral structure, the magnetic structure of the crystal is expected to induce chiral spin structure, i.e., *magnetic chirality* made out of *crystallographic chirality*. These magnets exhibit not only asymmetric magnetic anisotropy but also various types of novel magneto-optical phenomena such as non-linear magneto optical effect and magneto-chiral dichroism.[3)–5)] The materials of this category are not only of scientific interest, but they may also open a possible new window for new devices. To obtain chiral molecule-based magnets, the geometric symmetry such as chirality must be controlled in the molecular structure as well as in the entire crystal structure. In this paper, we describe recent results regarding

---

[*] Dedicated to Prof. Michinori Ōki on occasion of his 77th birthday.
[**] E-mail: kishine@mns.kyutech.ac.jp
[***] E-mail: kxi@hiroshima-u.ac.jp
[†] E-mail: D052650@hiroshima-u.ac.jp

magnetic structure and magnetic properties of molecule-based magnets with chiral structures from both experimental and theoretical viewpoints.

§2. Crystallographic chirality and magnetic chirality

Magnetic dipole moment and electric dipole moment are extremely important static objects in solid state physics. The investigation of properties and the search for magnetic materials that contain ferroelectric order materials are subjects of increasing interest.[6),7)] These multiferroic materials possess specific properties via the cross-effect of ferromagnetic nature and ferroelectric nature in the same phase. Generation of an asymmetric electric dipole field in the crystal is readily achieved by introduction of chirality. These classes of materials are not identical to ferroelectric materials, but they exhibit an asymmetric electric dipole field in the crystal or material. These materials are expected to possess unique magnetic anisotropy, field induced second harmonic generation and magneto-chiral optical effect due to the asymmetric electric dipole field. In this section, we argue the characteristic features of the chiral magnetic materials and their magnetic properties.

In terms of the magnetic structure, the main issue is the relationship between crystallographic chirality and magnetic chirality. The crystallographic chilarity gives rise to the asymmetric magnetic interactions and the single-ion anisotropy through the spin-orbital interactions. The most important asymmetric magnetic interaction in this context is the Dzyaloshinskii-Moriya (DM) interaction[8),9)] that violates the inversion symmetry in the spin space. Without the DM interaction, the left-handed and right-handed chiral magnetic structures are *degenerate* and the magnetic structure inevitably becomes achiral. Therefore, to fabricate matters, we need to control the crystallographic chirality via chemical synthesis, and then manipulate resultant asymmetric exchange interactions. Bearing this in mind, it is apparent that the crystallographic chirality is NOT always accompanied by the magnetic chirality. So far, we have the following two promising candidates for the chiral magnetic structure:
Case A: chiral spin ordering occurs along a crystallographic chiral spiral, or
Case B: chiral spin ordering occurs along a crystallographic axis.
In the case A, magnetic ions are located in a line along with the spiral (see Fig. 9 as a real example). In the case B, the crystallographic chirality is not a direct origin of the magnetic chirality (see Fig. 6 as a real example). We here discuss the two cases with emphasis on the microscopic origin of the magnetic chirality and its physical consequence. These cases are pictorially shown in Fig. 1.

2.1. *Chiral spin ordering along a crystallographical spiral*

We consider the case A where the magnetic ions are located in line with the spiral. It is apparent that the nearest-neighbor ferromagnetic exchange interaction alone cannot stabilize the magnetic chirality. The dipolar interaction and the DM interaction in the direction of the spiral axis are needed. This situation is materialized in a magnetic crystal with the space group PN_1. To see this, we write a spin
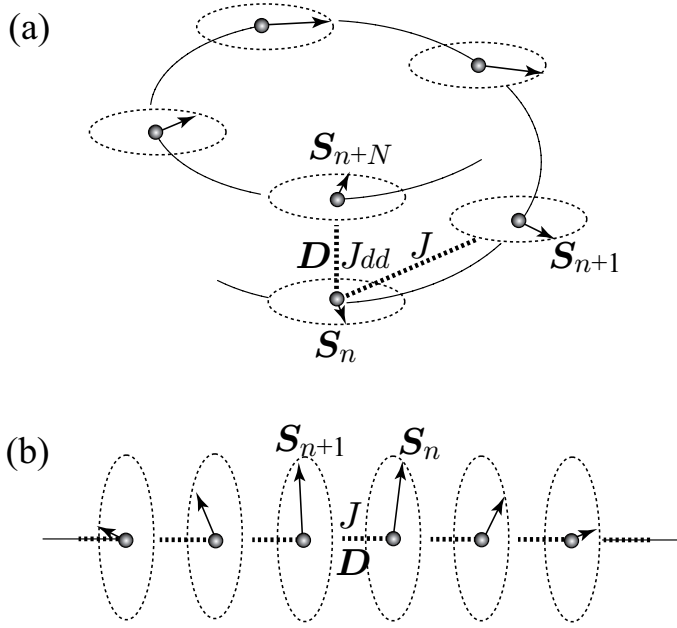
Fig. 1. (a) Chiral spin ordering occurs along a crystallographic spiral with N-fold symmetry (the case of $N = 6$ is shown.), and (b) chiral spin ordering occurs along a crystallographic axis.

Hamiltonian,

$$H = -J \sum_n \boldsymbol{S}_n \cdot \boldsymbol{S}_{n+1} + \boldsymbol{D} \cdot \sum_n \boldsymbol{S}_n \times \boldsymbol{S}_{n+N}$$

$$+ (g\mu_B)^2 \sum_n \frac{1}{d^3} \left\{ \boldsymbol{S}_n \cdot \boldsymbol{S}_{n+N} - 3 \frac{(\boldsymbol{d} \cdot \boldsymbol{S}_n)(\boldsymbol{d} \cdot \boldsymbol{S}_{n+N})}{d^2} \right\}, \qquad (2\cdot1)$$

where the first term represents the nearest-neighbor ferromagnetic coupling with strength J, the second term represents the DM interaction (with strength $\boldsymbol{D}$), the third term represents the dipolar interaction. Emergence of the DM term is a direct consequence of the inversion symmetry breaking in the spiral axis direction. Assuming all the spins to lie inside the plane perpendicular to the spiral axis and treating the spin variable as a classical vector, the energy per spin per site is written as

$$E/NS^2 = -J\cos(\theta) + J_{\mathrm{dd}}\cos(N\theta) + D\sin(N\theta), \qquad (2\cdot2)$$

where $\theta = \theta_{n+1} - \theta_n$ denotes an angle spanned by the nearest-neighbor spins and $J_{\mathrm{dd}} = (g\mu_B)^2/d^3$. In Fig. 2(a), we show the energy profile as a function of θ with $N = 6$. A positive and negative θ correspond to the left-handed and right-handed magnetic chirality, respectively. It is clearly seen that the D-term lifts the degeneracy of the two energy minima and picks out only one chirality. In Fig. 2(b), we show the pitch of the spin screw, $2\pi/\theta_0$ with θ_0 being the angle that minimizes $(2\cdot2)$.

2.2. Chiral spin ordering along a crystallographic axis and chiral spin soliton

Next we consider the case B, where chiral spin ordering occurs along a crystallographic axis (we take this as z-axis). This situation may be materialized in a
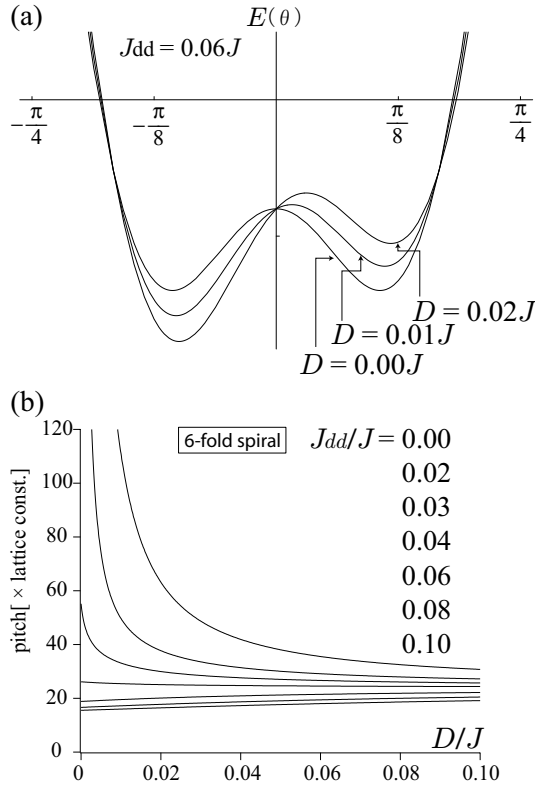
Fig. 2. (a) The energy profile as a function of the angle θ spanned by the nearest-neighbor spins, and (b) the pitch length of the screw spin structure. We set $N = 6$ (corresponding to the 6-fold symmetry).

magnetic crystal where the DM vector survives along only one crystallographic axis and is suitably described by the Hamiltonian

$$\mathcal{H} = -J \sum_n \boldsymbol{S}_n \cdot \boldsymbol{S}_{n+1} + \boldsymbol{D} \cdot \sum_n \boldsymbol{S}_n \times \boldsymbol{S}_{n+1} - 2\mu_B H \sum_n S_n^x, \qquad (2\cdot3)$$

where the first and second terms respectively represent ferromagnetic exchange interaction, the DM interaction between the nearest-neighbor spins along the screw axis in Fig. 1. The Zeeman term by the transverse magnetic field is added. The most prominent feature of this case may be the emergence of the C-IC transition and the concomitant chiral spin soliton lattice formation. As for the C-IC transition in spin systems, only a few real examples have been known so far. More than two decades ago, the helical spin structure due to the coexistence of the ferromagnetic exchange and the DM interactions was found in $Cr_{1/3}NbS_2$.[10] At that time, however, the aspect of the C-IC transition was not addressed. Rather recently, Zheludev et al.[11] reported a C-IC phase transition in the DM spiral antiferromagnet $Ba_2CuGe_2O_7$, where the transition is induced by an external magnetic field in the plane of spin rotation. Roessli et al.[12] reported that in copper metaborate CuB_2O_4 the interplay of the DM interaction and anisotropy leads to the formation of a magnetic soliton

lattice. Sukstanskii et al.[13] developed a theory for triangular helicoidal antiferromagnetic structures in $CsCuCl_3$ and investigated the soliton lattice formation. We believe that the chiral molecule-based magnets bring new facets of this long-standing issue.

Introducing the local polar coordinates as $\boldsymbol{S}_n = S(\sin\theta_0\cos\phi_n, \sin\theta_0\sin\phi_n, \cos\theta_0)$, the above Hamiltonian is transformed to the vector model,

$$\mathcal{H} = -S^2 \sum_n \left[\mathcal{J}\sin^2\theta_0\cos(\phi_{n+1}-\phi_n-\alpha) + J\cos^2\theta_0 \right]$$
$$-2\mu_B HS \sum_n \sin\theta_0\cos\phi_n \qquad (2\cdot4)$$

where $\mathcal{J} = \sqrt{J^2+D^2}$ and $\alpha = \tan^{-1}(D/J)$. The polar angle θ_0 spanned by the z-axis and the spin is assumed to be uniform. The direction of the uniform DM vector is assumed to be along the screw axis in Fig. 1. Now, the mean field states are either commensurate (C) phase ($\theta = \pi/2$, $\phi_n = 0$ for all the n) or incommensurate (IC) phase ($\theta = \pi/2$, $\phi_{n+1}-\phi_n = \alpha$ for all the n). In the IC phase, spins on the x-y plane form chiral screw with the screw axis being along the z-axis. Now, we concentrate on the case where the ground state is the IC chiral screw phase, i.e., the condition $D\,S^2 > \sqrt{\tilde{H}^2\,S^2 + 2\,\tilde{H}\,J\,S^3}$ is fulfilled, where $\tilde{H} = 2\mu_B H$. In this case, the Hamiltonian (2·4) becomes the *chiral XY model* described by

$$\mathcal{H}_{\text{ChiXY}} = -S^2\mathcal{J}\sum_n \cos(\phi_{n+1}-\phi_n-\alpha) - \tilde{H}S\sum_n \cos\phi_n. \qquad (2\cdot5)$$

It is now clear that the competition between the two terms of (2·5) may give rise to the commensurate-to-incommensurate (C-IC) phase transition and the concomitant soliton lattice formation in the vicinity of the transition below the second-order phase transition. Generally D is expected to be much smaller than J. Consequently, the zero-filed screw pitch angle given by $\alpha = \tan^{-1}(D/J)$ is quite small and the corresponding pitch, $(2\pi/\alpha) \times$ (lattice constant) becomes quite long as compared with the lattice constant. Because of this situation, taking continuum limit becomes legitimate. We thus have the energy along the z-axis as

$$E = \mathcal{J}S^2 \int dz \left[\frac{1}{2}\left(\frac{d\phi(z)}{dz}\right)^2 - \alpha\frac{d\phi(z)}{dz} - \beta\cos(\phi(z)) \right], \qquad (2\cdot6)$$

where $\beta = \tilde{H}/(\mathcal{J}S)$. Stationarity condition, $\delta E = 0$, gives the well-known sine-Gordon equation and the spin soliton configuration[14]

$$\sin\left(\frac{\phi(z)-\pi}{2}\right) = \text{sn}\left(\frac{\sqrt{\beta}}{k}z|k\right), \qquad (2\cdot7)$$

where $\text{sn}(x|k)$ is the Jacobi elliptic function with k ($0 < k^2 < 1$) being the elliptic modulus and the period of the chiral soliton lattice being given by

$$L = \frac{4kK(k)}{\sqrt{\beta}} = 4kK(k)\sqrt{\frac{\mathcal{J}S}{H}} \sim 4kK(k)\sqrt{\frac{JS}{H}}, \qquad (2\cdot8)$$
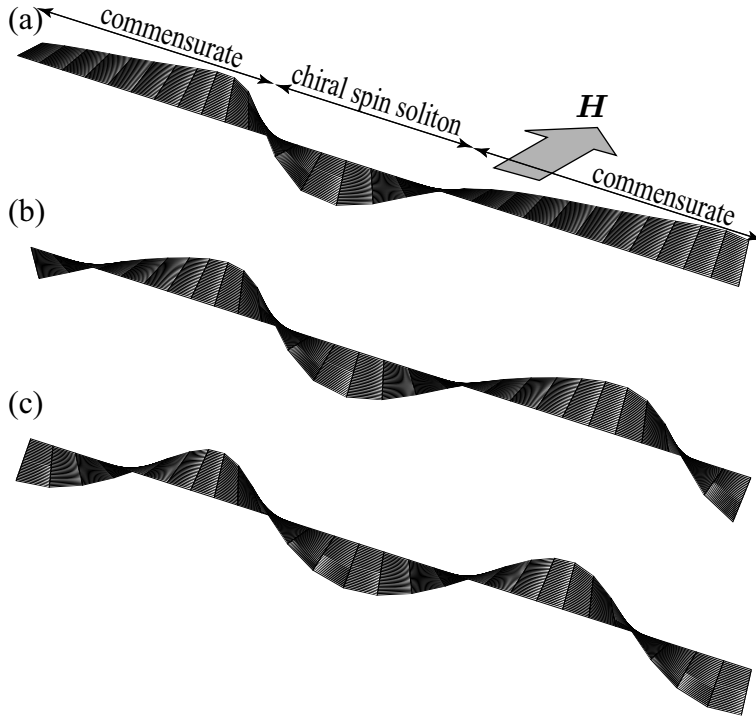
Fig. 3. Pictorial view of the spin textures in the chiral spin soliton lattice state over 1400 lattice units in the screw axis direction at the temperatures (a) and (b) indicated by the vertical arrows in Fig. 4, and (c) at $T = 0$.

with $K(k)$ being the complete elliptic integral of the first kind. In Fig. 3, we show a pictorial view of the spin texture in the chiral spin soliton lattice along the z-axis.

Now we consider the energy per unit length,

$$\mathcal{E} = \frac{\mathcal{J}S^2}{L} \int_{-L/2}^{L/2} \left[\frac{1}{2} \left(\frac{d\phi(z)}{dz} \right)^2 - \alpha \frac{d\phi(z)}{dz} - \beta \cos(\phi(z)) \right]. \tag{2·9}$$

Plugging (2·7) into (2·9), we have

$$\mathcal{E} = -2\beta \left(\frac{1}{k^2} + \frac{\pi\alpha}{2\sqrt{\beta}} \frac{1}{kK(k)} - \frac{2}{k^2} \frac{E(k)}{K(k)} \right), \tag{2·10}$$

where $K(k)$ and $E(k)$ are complete elliptic integrals of the first and second kinds, respectively. We find the value of the modulus k $(0 < k < 1)$ that gives the energy minimum as

$$\frac{\pi\alpha}{4\sqrt{\beta}} = \frac{E(k)}{k}. \tag{2·11}$$

The C-IC transition occurs at $k = 1(E(1) = 1)$, i.e.,

$$\frac{\pi\alpha}{4\sqrt{\beta_c}} = 1. \tag{2·12}$$

Now, to grapple with qualitative feature of the magnetization profile near the second-order phase transition, we consider the temperature dependence of the spin moment at a phenomenological level. The temperature dependence should be considered by treating the three-dimensional exchange coupling in a self-consistent manner. The stability of the soliton lattice formation in the three-dimensional environments should also be clarified. But we leave these problems for future investigation. At present, we simply replace S with the temperature-dependent one, $S(T) \sim S_0 \sqrt{(T_c - T)}$ with T_c being the second-order phase transition temperature. Then, the C-IC transition occurs at $T = T^*$ given by

$$S(T^*) = \frac{H}{\mathcal{J}} \left(\frac{4}{\pi \alpha} \right)^2 \sim \frac{H}{J} \left(\frac{4}{\pi \tan^{-1}(D/J)} \right)^2. \qquad (2\cdot13)$$

Then, the optimal elliptic modulus is given by

$$\sqrt{\frac{S(T)}{S(T^*)}} = \frac{E(k)}{k}. \qquad (2\cdot14)$$

The magnetization is computed by taking an average of the projection of the spin onto the magnetic field direction over the period of the soliton lattice. We have

$$\begin{aligned}
M(T) &= \frac{S(T)}{L} \int_{-L/2}^{L/2} \cos \phi(z) dz \\
&= 2\mu_B S(T) \left(-1 + \frac{2}{k^2} - \frac{2E(k)}{k^2 K(k)} \right). \qquad (2\cdot15)
\end{aligned}$$

For example, an external field with strength of 5 Oe gives $\tilde{H}/J \sim 10^{-5}$ and $\alpha \sim D/J = 0.01$. In Fig. 4, we show the numerical result. The C-IC transition gives
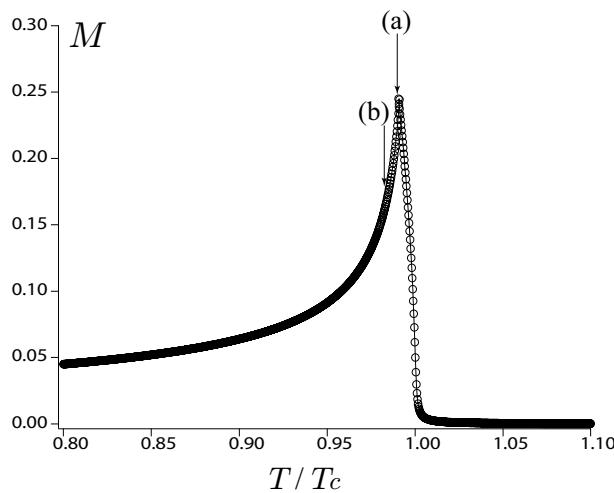
Fig. 4. Theoretical result for the temperature dependence of the magnetization for the case of $S_0 = \frac{5}{2}$, $\tilde{H}/J = 1.0 \times 10^{-5}$, and $\alpha \sim D/J = 0.01$.

quite a sharp peak just below T_c. Although the present argument is quite a rough phenomenology, the characteristic peak structure is eventually found in the compound as explained below. In Fig. 4, we see that the magnetization continues to decrease toward $T = 0$. This situation is easily explained by the single-ion anisotropy (SIA), that has been ignored so far. At low temperature, the effect of the SIA becomes crucial and all the spins are eventually aligned to the easy-axis direction. Full temperature dependence of the magnetization with the SIA being included will be discussed elsewhere in detail.

§3. Materials

The major strategy relating to crystal design for magnetic materials exhibiting higher ordering temperature and spontaneous magnetization involves generation of an extended multi-dimensional array of paramagnetic metal ions with bridging ligands. The cyanide-bridged Prussian-blue systems are well known as the most suitable method for this end. These systems are generally obtained as bimetallic assemblies with a three-dimensional cubic cyanide network by the reaction of hexacyanometalate $[M^{III}(CN)_6]^{3-}$ with a simple metallic ion M^{II}.[15]–[18] Extensive research has lead to the production of a material displaying magnetic ordering at T_c as high as 372 K.[19] On the one hand, the attention of some chemists has been focused on specific coordination sites around M^{II} in this system. Ōkawa and Ohba have found that some organic molecules can be incorporated into this system as chelating or bidentate ligand L to M^{II}.[20],[21] The incorporation of such a ligand leads to the blockade of some coordinated linkages to M^{II} of cyanide groups in $[M^{III}(CN)_6]^{3-}$. It follows that various novel structures have been obtained in this system, depending on the organic molecule. This method affords the possibility of crystal design in cyanide-bridged systems. In this section, we will describe the crystal design toward a chiral magnet utilizing a cyanide-bridged system; additionally, several examples are presented.

3.1. *Crystal design*

When chiral molecule-based magnets exhibiting higher ordering temperature and spontaneous magnetization are constructed, the chirality in the entire crystal structure as well as the high dimensionality of the extended arrays must be maintained.[22]–[26] It is more convenient for the cyanide-bridged systems to circumvent these difficulties in order to construct higher-T_c chiral magnets. Some chiral diamine ligands serve as candidates for the chiral source in the entire crystal structure of this system. In other words, a target magnetic compound can be generated by the reaction between a hexacyanometalate $[M^{III}(CN)_6]^{3-}$ and a mononuclear complex $[M^{II}(L)_n]$ based on chiral diamines, as shown in a scheme below (see Fig. 5). It notes, however, the combination of M^{II} and M^{III} in the stage of crystallization must be known, which generates ferromagnetic interaction through M^{III}-CN-M^{II}, in order to obtain a ferromagnet. This method holds many possibilities with respect to obtaining various chiral magnets via alteration of the component substances.

$$\left[\begin{array}{c} \text{Cr(CN)}_6 \end{array} \right]^{3-} \quad \left[\begin{array}{c} \text{Mn} \end{array} \right]^{2+}$$

) * = Chiral organic ligand
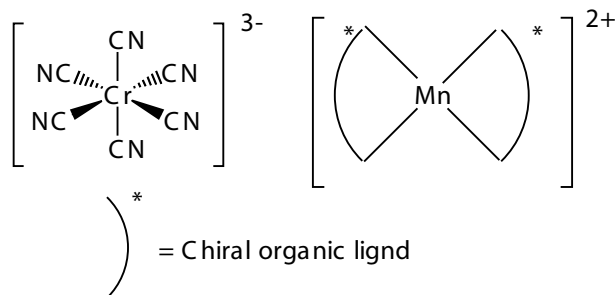
Fig. 5. Crystal design for chiral magnets by substituting cyano group with chiral ligand.

3.2. *Chiral molecule-based magnets made by Cr^{III} and Mn^{II}*

Structural characterized green needles: $[Cr(CN)_6][Mn(S$ or $R)$-pnH$(H_2O)]H_2O$ and yellow needles: $K_{0.4}[Cr(CN)_6][Mn(S)$-pn$](S)$-pnH$_{0.6}$: $((S)$-pn $= (S)$-1,2-diaminopropane) were obtained by the reaction among $K_3[Cr(CN)_6]$, $Mn(ClO_4)_2$, $(R$ or $S)$-pn·2HCl and KOH.

3.2.1. The green needle: $[Cr(CN)_6][Mn(S$ or $R)$-pnH$(H_2O)]H_2O$

The green needle crystallizes in the non-centrosymmetric $P2_12_12_1$ space group. X-ray crystal structure analysis reveals that this compound consists of two-dimensional bimetallic sheets. Each $[Cr(CN)_6]^{3-}$ ion involves four cyanide groups in order to bridge with four adjacent Mn^{II} ions within the *ab* plane. (Fig. 6) In addition to one Mn^{II} and one $[Cr(CN)_6]^{3-}$ ions, an asymmetric unit in this crystal also associates with one mono-protonated $(S$ or $R)$-diaminopropane $((S$ or $R)$-pnH) and two water molecules. An octahedron around a Mn^{II} ion is completed with one $(S$ or $R)$-pnH and one water molecules which separate adjacent bimetallic sheets along the *c*-axis. The shortest and the second shortest inter-sheet metal separation are observed between the Cr and Mn atoms (the distances are 7.31 and 7.77 Å, respectively), in contrast, the shortest inter-sheet homo-metal contacts are beyond 8 Å. This observation suggests that the ferromagnetic interaction operates preferentially between bimetallic sheets.

The temperature dependence of magnetic susceptibility shows the antiferromagnetic interaction operates between the adjacent Cr^{III} and Mn^{II} ions through cyanide bridges above 140 K. The abrupt increase of $\chi_{mol}T$ value around 40 K suggests the onset of three-dimensional magnetic ordering. As shown in Fig. 7, the magnetization (M) increases sharply with an applied field and is saturated rapidly. The saturation magnetization value of $M_S = 2\mu_B$ is in close agreement with the theoretical value of antiferromagnetic coupling between Cr^{III} and Mn^{II} ions. The hysteresis loop (the remnant magnetization of 1800 emu G mol^{-1} and the coercive field of 10 Oe) was observed at 5K, suggesting a soft magnetic behavior.[23), 24)]

In Figs. 8(a) and (b), we show the temperature dependence of the magnetization when the fields are parallel to the *a*-axis and *b*-axis, respectively. Both the field cooled (FC) and the zero field cooled magnetization measurements (ZFC) with a low applied field (5 G) in the temperature range from 2 K to 50 K display a long-range magnetic ordering below 38 K. It is now clearly seen that the steep cusp structure appears *only*

Chiral molecule
(*R*)- 1,2-diaminopropane

N

O

C

Mn
Cr

c

a   b
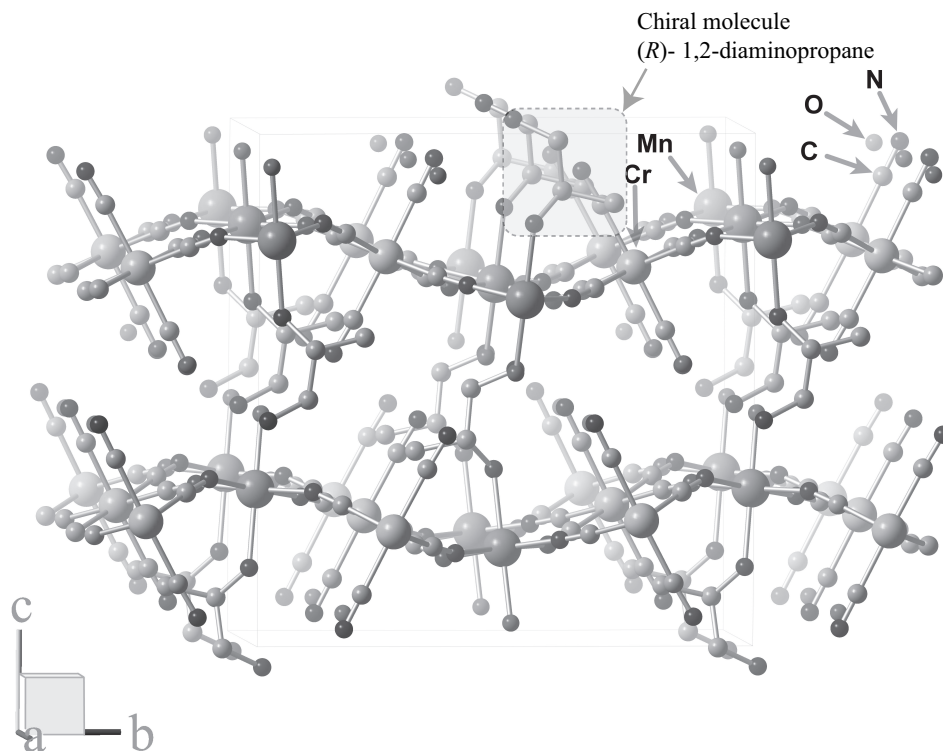
Fig. 6.   Crystal structure of $[Cr(CN)_6][Mn(S)-pnH(H_2O)](H_2O)]$.

when the field is perpendicular to the *a*-axis, i.e., perpendicular to the expected screw axis. This experimental finding is quite consistent with the theoretical prediction of the magnetization curve based on the chiral spin soliton picture (Fig. 4). We may say that we have a strong support for the chiral screw spin structure below 38 K.
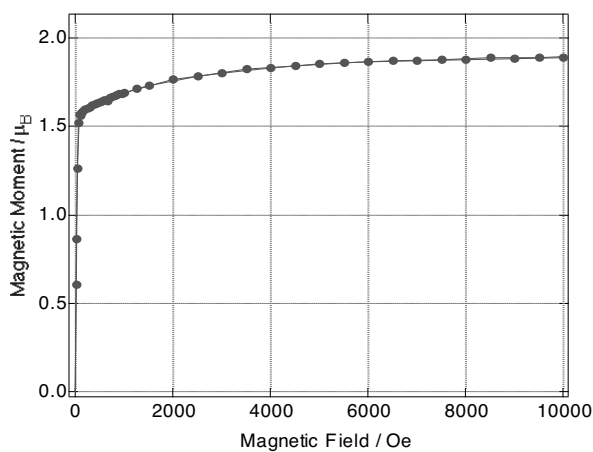
Fig. 7.   Field dependence of magnetization of $[Cr(CN)_6][Mn(S)-pnH(H_2O)](H_2O)]$ at 5 K.
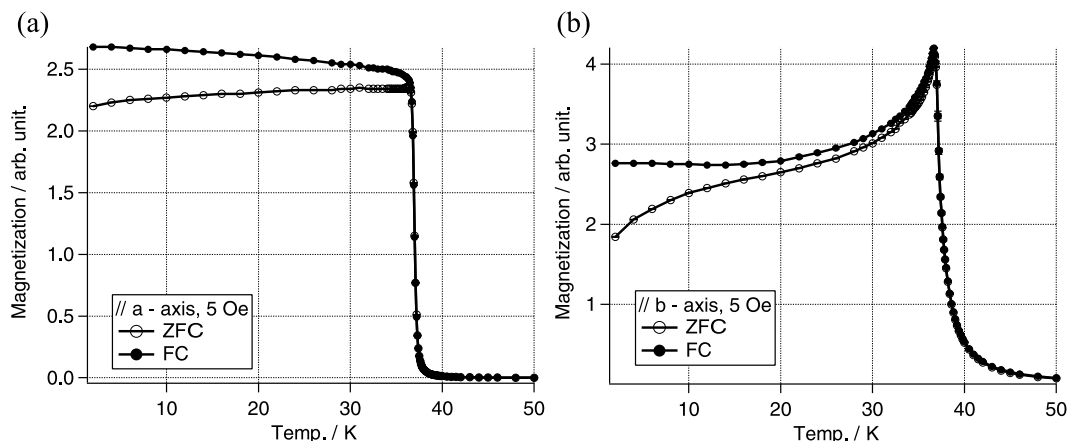
Fig. 8. Temperature dependence of the magnetization of $[Cr(CN)_6][Mn(S)-pnH(H_2O)](H_2O)]$ in low field (5 Oe). The fields are parallel to the (a) *a*-axis and (b) *b*-axis, respectively.

3.2.2. The yellow needle: $K_{0.4}[Cr(CN)_6][Mn(S)-pn](S)-pnH_{0.6}$

The yellow needle crystallizes in the chiral $P6_1$ space group. X-ray crystallography reveals that this compound consists of a three-dimensional chiral polymer (Fig. 9). Each $[Cr(CN)_6]^{3-}$ ion utilizes two cyanide groups to bridge two Mn^{II} ions forming helical loops along the *c*-axis, whereas two of the remaining four cyanide groups connect the adjacent loops. The shortest intra- and interloop Mn-Cr distances are 5.21 and 5.31 Å, respectively. The Mn^{II} ion exists in an octahedral environment with four cyanide groups of four distinct $[Cr(CN)_6]^{3-}$ and two nitrogen atoms of (S)-pn. In this crystal, two kinds of counter ion are included so as to maintain overall neutrality. One is a potassium ion and the other is mono-protonated diaminopropane (S)-pnH: the site occupancy of which is 0.4: 0.6, respectively. These counter ions are located within the cavity of helical loops.

In this case, the temperature dependence of magnetic susceptibility shows the antiferromagnetic interaction operates between the adjacent Cr^{III} and Mn^{II} ions through cyanide bridges above 110 K. The abrupt increase of $\chi_{mol}T$ value around 60 K suggests the onset of three-dimensional magnetic ordering. Both field-cooled magnetization (FCM) and the zero-filed-cooled magnetization (ZFCM) curves show an abrupt increase in M below 53 K (Fig. 10). The field dependence of magnetization at 5 K also reveals that the magnetization (M) is saturated rapidly in the presence of an applied field (Fig. 11). The saturation magnetization $M_S = 2\mu_B$ is close to the theoretical value of antiferromagnetic coupling between Cr^{III} and Mn^{II} ions. The hysteresis loop (the remnant magnetization of 30 emu G mol^{-1} and the coercive field of 12 G) was observed at 2 K, suggesting a soft magnetic behavior.[25] The present compounds provide proof that the cyanide-bridged system affords much potential ability in the design of molecule-based materials. Utility of chiral ligands in the synthesis of compounds based on the cyanide-bridged system leads to two- and three-dimensional chiral magnetic networks. These systems are candidates for asymmetric magnetic anisotropy, as well as for magneto-optical properties including magneto-
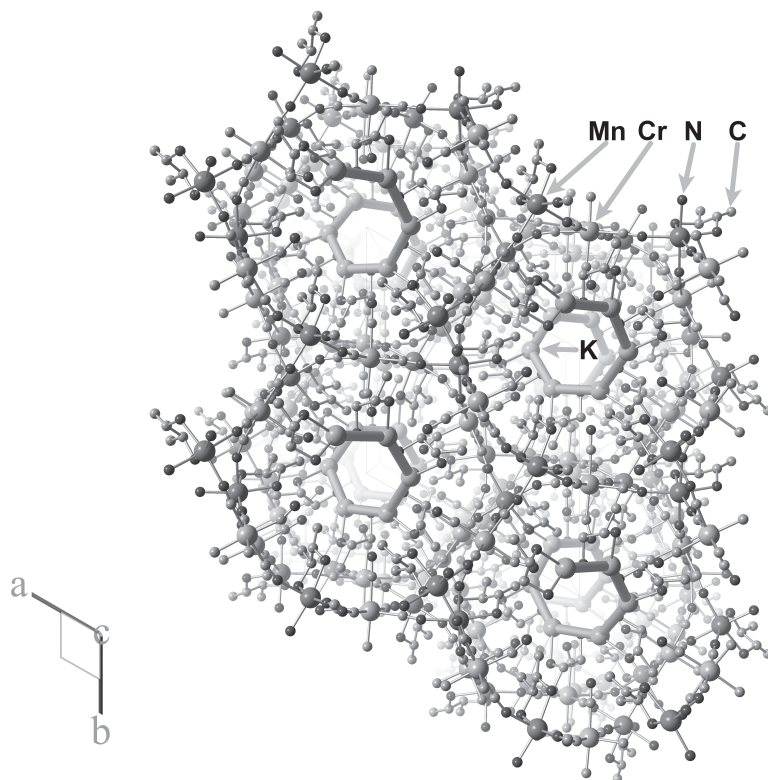
Fig. 9.   Crystal structure of $K_{0.4}[Cr^{III}(CN)_6][Mn^{II}(S)\text{-pn}](S)\text{-pnH}_{0.6}$.

chiral dichroism (MChD). This phenomenon is attributable to the ease with which these systems modulate optical activity, magnetization, ordering temperature and crystal color by changing paramagnetic metal ions and organic chiral ligands.

§4.   Conclusion

Notable features of molecule-based magnets lie in their flexible designability and transparency. So far, a novel category of materials suitable for chiral magnets has been successfully fabricated on purpose for application in the field of molecule-based magnetic materials. The interplay of crystallographic and magnetic chirality may play a key role to provide new optical phenomena such as magnetization-induced non-linear optical effect and magneto-chiral optical effect. The materials of this category are not only of keen scientific interest, but they may also open a possible new window for new device synthesis and fabrication. In this paper, we described some recent progress regarding magnetic structure and magnetic properties of molecule-based magnets with chiral structures from both experimental and theoretical viewpoints. We believe that the chiral molecule-based magnets certainly carve out new facets of a long-standing history of magnetism and magnetic materials.
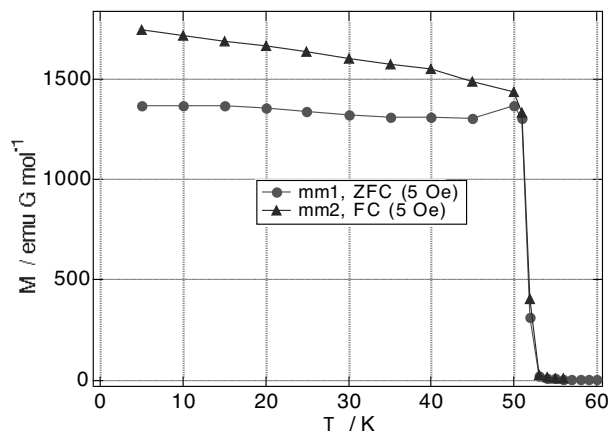
Fig. 10. Temperature dependence of magnetization of $K_{0.4}[Cr^{III}(CN)_6][Mn^{II}(S)\text{-pn}](S)\text{-pnH}_{0.6}$ in low field (5 Oe).
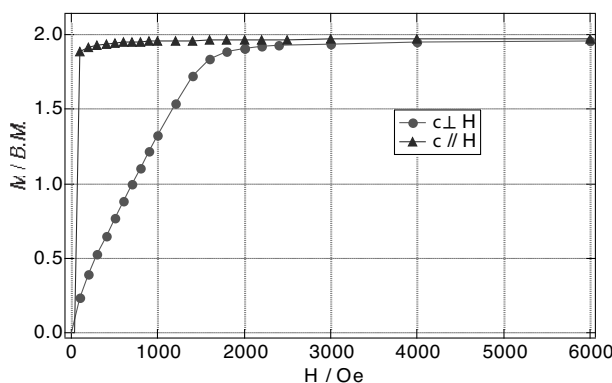
Fig. 11. Field dependence of magnetization of $K_{0.4}[Cr^{III}(CN)_6][Mn^{II}(S)\text{-pn}](S)\text{-pnH}_{0.6}$ at 5 K.

Acknowledgements

References

1) C. Bellitto and P. Day, J. C. S. Chem. Comm. No. 12 (1978), 511.
2) P. Day, in *Supramolecular Engineering of Synthetic Metallic Materials Conductors and Magnets,* NATO ASI Series vol. C518, ed. J. Veciana, C. Rovira and D. B. Amabilino (Kluwer Academic Publishers, New York, 1999), p. 253.
3) G. Wagniere and A. Mejer, Chem. Phys. Lett. **93** (1982), 78.
4) L. D. Barron and J. Vrbancich, Mol. Phys. **110** (1984), 546.
5) G. L. J. A. Rikken and E. Raupach, Nature **390** (1997), 493.
6) M. Fiebig, Th. Lottermoser, D. Fröhlich, A. V. Goltsev and R. V. Pisarev, Nature **419** (2002), 818.
7) N. A. Hill, J. Phys. Chem. B **104** (2000), 6694.

8) I. E. Dzyaloshinskii, Sov. Phys. -JETP **5** (1957), 1259.
9) T. Moriya, Phys. Rev. **120** (1960), 91.
10) T. Moriya and T. Miyadai, Solid State Commun. **42** (1982), 209.
11) A. Zheludev, S. Maslov, G. Shirane, Y. Sasago, N. Koide and K. Uchinokura, Phys. Rev. B **57** (1998), 2968.
12) B. Roessli, J. Schefer, G. A. Petrakovskii, B. Ouladdiaf, M. Boehm1, U. Staub, A. Vorotinov and L. Bezmaternikh, Phys. Rev. Lett. **86** (2001), 1885.
13) A. L. Sukstanskii, E. P. Stefanovskii, S. A. Reshetnyak and V. N. Varyukhin, Phys. Rev. B **61** (2000), 8843.
14) P. G. de Gennes, Solid State Commun. **6** (1968), 163.
15) For example, T. Mallah, S. Thiébaut, M. Veldaguer and P. Villet, Science **262** (1993), 1554.
16) S. Ferlay, T. Mallah, R. Ouahés, P. Veillt and M. Verdaguer, Nature **378** (1995), 701.
17) W. R. Entley and G. S. Girolami, Science **268** (1995), 397.
18) S. Ferlay, T. Mallah, R. Ouahés, P. Veillt and M. Verdaguer, Inorg. Chem. **38** (1999), 229.
19) S. M. Holmes and G. S. Girolami, J. Am. Chem. Soc. **121** (1999), 5593.
20) M. Ohba, N. Usuki, N. Fukita and H. Ōkawa, Angew. Chem. Int. Ed. **38** (1999), 1795.
21) M. Ohba and H. Ōkawa, Coord. Chem. Rev. **198** (2000), 313.
22) H. Imai, K. Inoue, K. Kikuchi, Y. Yoshida, M. Ito, T. Sunahara and S. Onaka, Angew. Chem. Int. Ed. **43** (2004), 5618.
23) K. Inoue, K. Kikuchi, M. Ohba and H. Ōkawa, Angew. Chem. Int. Ed. **42** (2003), 4810.
24) A. Hoshikawa, T. Kamiyama, A. Purwanto, K. Oishi, W. Higemoto, T. Ishigaki, H. Imai and K. Inoue, J. Phys. Soc. Jpn. **73** (2004), 2597.
25) K. Inoue, H. Imai, P. S. Ghalsasi, K. Kikuchi, M. Ohba, H. Ōkawa and J. V. Yakhmi, Angew. Chem. Int. Ed. **48** (2001), 4242.
26) H. Kumagai and K. Inoue, Angew. Chem. Int. Ed. **38** (1999), 1601.